Volume 7
Number 1
12 January 2026
Pages 1–666

# Materials Advances

rsc.li/materials-advances

ISSN 2633-5409

ROYAL SOCIETY OF CHEMISTRY

**PAPER**

Yuming Zhao *et al.*

Nanocomposite of eugenol/polysiloxane/graphene oxide as an efficient anticorrosion and anti-biofouling additive for marine epoxy coatings

Materials Advances

ROYAL SOCIETY OF CHEMISTRY

PAPER

View Article Online
View Journal | View Issue



Cite this: *Mater. Adv.*, 2026, 7, 214

# Nanocomposite of eugenol/polysiloxane/graphene oxide as an efficient anticorrosion and anti-biofouling additive for marine epoxy coatings

Nadia Khan,[a] Zahra A. Tabasi,[b] Leila Nazari,[a] Baiyu Zhang,[b] Talia J. Stockmann[a] and Yuming Zhao *[a]

A novel nanocomposite, **Eu-PMHS-GO**, was synthesized through a Pt-catalyzed hydrosilylation of polymethylhydrosiloxane (**PMHS**) with eugenol (**Eu**), followed by esterification with graphene oxide (**GO**). A marine epoxy resin was then modified with **Eu-PMHS-GO** as a dual-function additive for enhanced anticorrosion and anti-biofouling properties. Our studies demonstrated that **Eu-PMHS-GO** significantly improved the hydrophobicity and mechanical strength of the epoxy coatings, with optimal performance observed at 0.001 wt% additive loading. The modified coatings exhibited superior anticorrosion performance, maintaining high water repellency and corrosion resistance ($R_{corr}$ = 2.73 × $10^8$ Ohm) even after 30 days of immersion in seawater. Additionally, the incorporation of **Eu-PMHS-GO** inhibited the adhesion of marine microorganisms, including the diatom *Phaeodactylum tricornutum* and two bacterial strains, *Bacillus subtilis* and *Synechococcus* sp. At low additive loadings (0.001–0.05 wt%), the epoxy coatings showed high anti-algal and anti-bacterial adhesion efficiencies. However, at higher loadings (>0.1 wt%), the performance decreased sharply, which is attributed to increased aggregation of **Eu-PMHS-GO** in the epoxy coating layer. This comprehensive study not only demonstrates the applicability of **Eu-PMHS-GO** as an efficient, multifunctional additive in marine coating technology, but contributes a novel approach for addressing the practical limitations of current marine coatings through the development and implementation of high-performance nanocomposite additives.

Received 12th September 2025,
Accepted 29th October 2025

DOI: 10.1039/d5ma01048a

rsc.li/materials-advances



## Introduction

Marine environments present a challenging combination of factors, including corrosion,[1–3] biofouling,[4,5] and mechanical stress, which significantly reduce the lifespan and performance of materials used in maritime industries. Traditional protective coatings, while effective to some extent, often suffer from limitations such as poor environmental stability, low durability, and restricted functionality. Recent advancements in nanotechnology have introduced graphene-based nanocomposites as promising solutions for marine coatings,[6–11] offering superior performance due to their unique physicochemical properties. Graphene (**Gr**) is a 2-dimensional carbon nanomaterial that exhibits many advantageous properties for coating application, including excellent mechanical strength, chemical inertness, electrical conductivity, and thermal stability.[12–17] In recent years, graphene and its derivatives have been widely studied as functional additives for enhancing the performance of polymer-based coatings.[7,8,18] Graphene derivatives such as graphene oxide (**GO**)[19–22] and reduced graphene oxide (**rGO**)[23,24] exhibit improved dispersion and adhesion in various polymer matrices, resulting in uniform and stable coatings.[11,25–28] When incorporated into marine coatings, they can be integrated into composite systems to extend the diffusion paths (*e.g.*, tortuosity) of corrosive media and inhibit electrochemical reactions at the metal surface.[29,30] Moreover, certain oxygen-containing functional groups in **GO** and **rGO** allow for further chemical modifications to bring about new properties such as self-healing, anti-biofouling,[31–34] anti-icing,[35–38] and enhanced UV resistance,[39–41] which further enhance the performance of coatings in harsh environment.

Recent research has also focused on hybridizing graphene with other environmentally friendly (green) functional components.[42] Graphene-based materials are eco-friendly and can reduce the reliance on traditional corrosion inhibitors or heavy-metal-based coatings. These nanocomposites capitalize on the synergistic effects of graphene's impermeability and the special properties of certain functional additives to develop coatings with dual or even multifunctional roles. Polysiloxanes (also known as silicones)

[a] *Department of Chemistry, Memorial University of Newfoundland, St. John's, NL A1C 5S7, Canada. E-mail: yuming@mun.ca; Fax: +1 709 864 3702; Tel: +1 709 864 8747*
[b] *Faculty of Engineering and Applied Science, Memorial University of Newfoundland, St. John's, NL A1B 3X5, Canada*

are environmentally friendly polymers that have gained significant attention in coating technology due to their uniquely combined physical and chemical properties.[43–45] Polysiloxanes are primarily made of Si–O bonds, showing high hydrophobicity and low surface energy that deliver efficient antifouling and anti-icing performances.[46–48] In a coating layer, they can effectively create a water-repellent barrier to prevent the penetration of moisture and corrosive agents, thereby enhancing anticorrosion performance.[49–51] Additionally, polysiloxanes exhibit excellent thermal and chemical stability, which are beneficial for long-term durability in harsh marine environments.[51] In antifouling applications, their low surface energy inhibits the adhesion of microorganisms, algae, and other fouling organisms, reducing biofilm formation and fouling accumulation.[52–55]

Like **GO** and **rGO**, polysiloxanes can also be chemically modified to incorporate functional groups, such as eugenol (**Eu**) or other bioactive moieties, to enhance their antifouling properties without compromising their mechanical integrity. This versatility, combined with their environmental compatibility and ease of application, makes polysiloxanes promising materials for developing advanced marine coatings that address both corrosion and fouling challenges effectively. In our previous work, a family of **Eu**-modified polysiloxanes was developed and characterized, demonstrating their capacity to act as efficient anticorrosion additives for marine epoxy resin coatings.[56]

Derived from natural sources such as clove oil or lignin, **Eu** is a renewable and sustainable alternative to fossil-based materials.[57–59] In addition to its versatile reactivity, which allows the synthesis of a wide range of functional derivatives, the polar methoxy and hydroxy groups in **Eu** facilitate the formation of strong chemical bonds with substrates, resulting in **Eu**-modified coatings with strong adhesion. These properties make **Eu** a favored building block in the development of advanced coating materials. For example, Pang *et al.* prepared a nanocomposite containing **Eu**–polysiloxane–polycarbonate mixed with graphene, which exhibited enhanced mechanical strength, thermal stability, barrier properties, and hydrophobicity.[60] Additionally, **Eu** exhibits intrinsic antimicrobial activity,[61–63] making it useful for enhancing the bioactive properties of coatings, particularly in applications requiring hygiene and resistance to microbial growth. Furthermore, the use of **Eu** aligns with green chemistry principles, minimizing the carbon footprint and reducing reliance on hazardous reagents.[57]

Given that there have been no studies so far combining **Eu** with polysiloxane and **GO** for multi-functional coatings, in this work, we designed and investigated a novel nanocomposite composed of these three functional components covalently linked to one another. This nanocomposite integrates the advantageous properties of each nanoscale building block and was expected to exhibit enhanced protective performance when dispersed in polymer coatings. As illustrated in Fig. 1, the anticorrosion and antifouling performance of conventional polymer coatings can be improved by incorporating this nanocomposite as a multifunctional additive. The working mechanisms include: (i) enhanced surface hydrophobicity that protects the coating from corrosive and biofouling agents, (ii) blockage of water penetration pathways within the polymer matrix, and (iii) reinforcement of the coating's

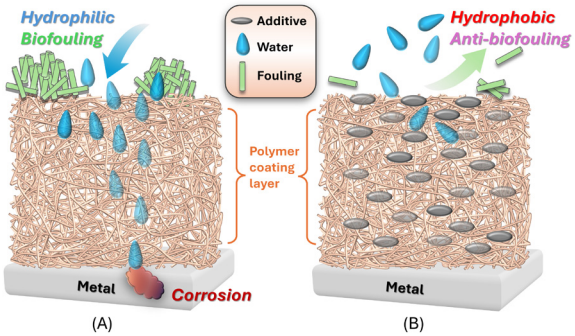


Fig. 1 Comparison of the protective effects of (A) a conventional polymer coating and (B) a polymer coating dispersed with multifunctional additives.

structural integrity and surface adhesion due to the polar effects of **Eu**. This study aims to synthesize **Eu-PMHS-GO** and evaluate its dual functionality (*i.e.*, anticorrosion and anti-biofouling) in epoxy coatings under marine conditions.

## Experimental section

### Materials

Natural graphite flake (size $\leq 1$ μm), polymethylhydrosiloxane (**PMHS**, $M_n$ = 1700–3500 g mol$^{-1}$), eugenol (**Eu**), thionyl chloride, 4-dimethylaminopyridine (DMAP), and chloroplatinic acid ($H_2PtCl_6$) were purchased from Sigma–Aldrich. All solvents were of reagent grade and used as received. Unmodified liquid epoxy resin (a diglycidyl ether of bisphenol A, EPON 828) and a polyamide curing agent (EPIKURE 3115) were provided by Hexion Inc., Ohio, USA (detailed information can be found from **https://www.hexion.com**). Steel test panels (Q-PANEL QD-36) were procured from Q-Lab Corp (**https://www.q-lab.com**), which were thoroughly rinsed with acetone and then dried in a desiccator for 24 hours prior to use.

*Bacillus subtilis* (or *B. subtilis*, a Gram-positive bacterium) was obtained from the NRPOP lab, Memorial University of Newfoundland, St. John's, Newfoundland and Labrador, Canada. *Synechococcus* sp. SR RCC2385 (cyanobacterium) was obtained from the Roscoff Culture Collection (RCC) at Station Biologique de Roscoff, France. *Phaeodactylum tricornutum* (or *P. tricornutum*) CCAP 1052/1A strain was obtained from the Culture Collection of Algae and Protozoa (CCAP), Scotland, UK.

### Instrumentation

Fourier transform infrared (FTIR) spectra were recorded with a PerkinElmer Spectrum 100 FTIR spectrometer in an atmospheric environment using the attenuated total reflectance (ATR) method. Raman spectra were determined with an in Via Reflex spectrometer equipped with 532 nm laser excitation. Scanning electron microscopy combined with energy dispersive X-ray spectroscopic (SEM/EDX) analyses were conducted on a Hitachi S570 scanning electron microscope. Specimens were coated with a layer of gold (Au) prior to SEM imaging. Mechanical strength measurements were conducted with an Instron 5585H tensile testing machine. According to the GB/T1040.3-2006-B1 standard, sample plates were

clipped into standard shapes. The obtained values are the averages of three tests. Water contact angles (WCAs) were measured on a KRÜSS Drop Shape Analyzer–DSA25S (Krüss GmbH, Germany) from sessile deionized (DI) water drops in triplicate.

The corrosion performance of steel plates coated with epoxy resins was evaluated by electrochemical impedance spectroscopy (EIS) using a CHI6059 potentiostat (CH Instruments). Measurements were performed over a frequency range of 10 kHz to 0.1 Hz with a 10 mV perturbation amplitude, while monitoring open circuit potential (OCP). All EIS tests were conducted at room temperature, with each coating's OCP allowed to stabilize for 10–15 minutes prior to measurement. Test specimens consisted of neat and modified epoxy-coated steel plates (1 $cm^2$ exposed area) as working electrodes. A platinum (Pt) wire was used as the counter electrode, and Ag/AgCl as the reference electrode. Natural seawater served as the electrolyte, and measurements were performed within a grounded Faraday cage to minimize electromagnetic interference. EIS data were analyzed using ZView software (Scribner, LLC, USA) to obtain the electrochemical equivalent circuit (EEC).

Scanning electrochemical microscopy (SECM) was performed using an ElProScan potentiostat (Heka Elektronik) equipped with a 3-axis positioner. Measurements were conducted in negative feedback mode using a three-electrode configuration: a 25 μm diameter platinum ultramicroelectrode (UME) as the working electrode, a platinum wire counter electrode, and an Ag/AgCl reference electrode. The electrolyte contained ferrocene (0.9 mM in methanol) as a redox mediator and KCl (100 mM) as a supporting electrolyte. A 3D approach curve was recorded over a 300 × 300 $\mu m^2$ area by scanning the UME at a rate of 2 μm $s^{-1}$ and maintaining a tip-to-substrate distance of 10 μm to map surface activity and topography.

Visual confirmation of the microbial adhesion on the surface of epoxy coatings was carried out using a SWIFT SW380T Trinocular Compound Lab microscope equipped with a SWIFT 10-megapixel camera. Image analysis was performed using Swift Imaging 3.0 software.

# Methods

### Synthesis of Eu-PMHS-GO

Eugenol-functionalized polysiloxane (**Eu-PMHS**) was prepared using the Pt-catalyzed hydrosilylation method previously reported by Chen *et al.*[56] Graphene oxide (**GO**) was synthesized through a modified Hummers' method[64] described as follows: graphite flake (3.0 g) was added into concentrated $H_2SO_4$ (220 mL) mixed with $NaNO_3$ (1.5 g). The mixture was stirred in an ice–water bath for 2 h. To the cooled mixture was slowly added $KMnO_4$ (9.0 g) in two portions with temperature controlled below 15 °C. The resulting suspension was stirred at 35 °C for 24 h until a pasty brownish product of **GO** was formed. The reaction mixture was then poured onto ice and quenched by an aqueous $H_2O_2$ solution (34%, 25 mL). The **GO** product was collected through filtration followed by washing with DI water several times to remove residual acids and salts. The resulting **GO** was subsequently suspended in DI water and exfoliated by centrifugation (7000 rpm) for 30 min.

**GO** (0.29 g) was dispersed in DMF (20 mL) with the aid of a bath sonicator for 120 min. The resulting **GO** suspension was cooled with an ice–water bath under stirring, to which thionyl chloride ($SOCl_2$, 6 mL) was gradually added. The resulting mixture was then heated to 70 °C for 2 h to induce chlorination reactions on **GO**. The chlorinated intermediate was subjected to vacuum evaporation to remove solvents and unreacted $SOCl_2$. After this brief purification, the chlorinated **GO** was mixed with **Eu-PMHS** (0.68 g) and in dry THF (20 mL) and DMAP (0.24 g). The mixture was refluxed with continuous stirring at 80 °C for 24 h to generate **Eu-PMHS-GO** through esterification reactions. Afterward, the solid product of **Eu-PMHS-GO** was collected through suction filtration and then sequentially washed with hexanes and methanol to remove impurities. Finally, a purified **Eu-PMHS-GO** product (0.55 g) was obtained after drying under air at room temperature overnight.

### Preparation of Eu-PMHS-GO-modified epoxy resin coatings

Carbon steel plates Q235 with dimensions of 25 mm in width, 130 mm in length, and a thickness 0.8 mm were used as substrates for corrosion tests. The plates were successively polished with a series of sand papers (320–360 grit size), cleaned with acetone, and then dried under air at room temperature. The following is a representative procedure for preparing an epoxy resin coating containing a certain amount of **Eu-PMHS-GO** as additive and applying it onto a test carbon steel substrate: **Eu-PMHS-GO** (2.4 mg, 0.1 wt%) was added in 1-butanol (5 mL), and the mixture was probe-sonicated for 30 minutes to form a uniform dispersion. This mixture was then combined with epoxy resin (1.2 g), xylene (5 mL), and the curing agent (1.2 g) *via* the solution blending method. The resulting mixture was sonicated for another 30 min and then stirred at room temperature for 1 h. Next, the mixture was subjected to degassing in a vacuum oven at 29 °C for 2 h. The prepared **Eu-PMHS-GO**-modified epoxy resin was allowed to stand for another 30 min before being applied onto a steel plate by the brush coating method. The coated plate was placed in an oven at 60–70 °C for 3 days and then taken out for corrosion tests. The thickness of each coating layer was controlled between 45 ± 2 μm.

### Anticorrosion tests

Epoxy resin-coated steel panels were immersed in static natural seawater collected from the Ocean Science Center at Memorial University of Newfoundland (pH 8.0, salinity 3.5%) for a period of up to 90 days. The immersion tests were conducted at room temperature (23 °C). To evaluate the anticorrosion performance of the coatings, an X-shaped scratch was introduced into the surface of each specimen using a precision cutting tool. This artificial defect was designed to penetrate the coating and expose the underlying substrate, creating a localized area for accelerated corrosion. The dimensions of the scratch were carefully controlled to ensure consistency across all test specimens. The progression of corrosion was visually assessed and documented by high-resolution photographic imaging.

In addition to the scratch tests, EIS measurements were conducted on intact epoxy-coated samples immersed in

seawater for varying durations. These measurements were performed to investigate the corrosion mechanisms and evaluate the protective performance of the coatings over time under simulated marine conditions.

The erosion–corrosion resistance of the coatings was evaluated by exposing them to a highly aggressive slurry, simulating dynamic marine conditions. The test medium consisted of a 3.5 wt% NaCl aqueous solution containing 20 wt% suspended silica particles as the abrasive agent. Tests were conducted for durations of 24 and 72 h at a constant stirring rate of 500 rpm to assess the synergistic degradation from both mechanical wear and electrochemical corrosion. SECM operated in negative feedback mode was employed to probe the local electrochemical activity and topography of the coatings before and after erosion–corrosion exposure. This technique provided high-resolution mapping of the degradation process, enabling the precise identification of nascent defects, micro-cracks, and areas of compromised barrier integrity.

### Anti-algal adhesion test

An axenic culture of the marine diatom, *P. tricornutum* (strain CCAP 1052/1A), was cultivated in Guillard's *f*/2 medium enriched with silicate (*f*/2 + Si) for diatom growth. The medium was prepared using 500 mL of filtered and autoclaved local seawater, supplemented with *f*/2 vitamins and inorganic nutrients. The cultures were maintained in an incubator under cool white light at an irradiance of 35 μmol photons $m^{-2}$ $s^{-1}$, with a 16 : 8 h light : dark photoperiod and a constant temperature of 22 °C.

Glass slides coated with epoxy resin containing **Eu-PMHS-GO** additives at varying loading concentrations (0.000, 0.001, 0.005, 0.010, 0.050, 0.100, and 0.500 wt%) were sterilized by immersion in ethanol for 10 s and subsequently placed in Petri dishes. An aliquot of *P. tricornutum* culture (30 mL), with an initial cell concentration of $1 \times 10^5$ cells per mL, was added to each Petri dish. Cultures were kept at 30 °C for one week to allow biofilm formation. After incubation, the glass slides were carefully taken out of the Petri dishes and rinsed four times with Guillard's *f*/2 + Si medium to remove loosely attached algal cells. To preserve the attached algal biofilms, the slides were fixed with 2.5% glutaraldehyde for 2 h at 4 °C. The samples were then subjected to visualization and image analysis to quantify algal attachment as well as biofilm formation.

To assess the effectiveness of the coating in preventing biofouling, the number of clustered algal cells within a defined area on the glass slide was quantified. A cover slip with dimensions of 18 mm (length) × 18 mm (width) was used for cell counting. Four evenly distributed strips, each measuring 118 mm (length) × 18 mm (width), were analyzed to determine the number of cells attached to the coated glass slide. The density of clustered cells ($D$) was calculated using the following formula:

$$D = \frac{N}{A}$$

where $D$ is the density of the clustered cells, $N$ is the average number of clustered cells in each strip, and $A$ is the surface area of the strip.

### Anti-bacterial adhesion test

An axenic culture of *B. subtilis* (N3-1P strain) was cultured in Marine Broth 2216, prepared by suspending 37.4 g of marine broth powder in 1 L of distilled water. The mixture was heated with frequent agitation until boiling and kept for 10 min to ensure complete dissolution of the powder. The medium was then sterilized by autoclaving at 121 °C for 15 min. An aliquot of the prepared medium (200 mL) was used to inoculate *B. subtilis*, while the remaining medium was reserved for washing the coated glass slides. The bacterial culture was grown overnight in a Thermo Scientific MaxQ 4000 benchtop orbital shaker at 220 rpm and 30 °C.

*Synechococcus* sp. was cultured in PCR-S11 Red Sea medium, which was sterilized by autoclaving at 121 °C for 20 min. Cultures were kept in an incubator under cool white light at an irradiance of 20 μmol photons $m^{-2}$ $s^{-1}$ and a constant temperature of 22 °C. For bacterial subculturing, the culture was grown overnight in a Thermo Scientific MaxQ 4000 benchtop orbital shaker at 150 rpm and 22 °C. To ensure optimal growth conditions, the culture was transferred to fresh medium every four weeks.

Glass slides coated with epoxy resin incorporating **Eu-PMHS-GO** as additives were submerged in bacterial cultures for one week to evaluate their antifouling properties. Following incubation, the slides were imaged and analyzed using the same procedures described in the anti-algal adhesion test (see above).

## Results and discussion

### Synthesis and characterization of Eu-PMHS-GO

The synthetic route to **Eu-PMHS-GO** is illustrated in Fig. 2. The initial reaction involved the hydrosilylation of polymethylhydrosiloxane (**PMHS**) with eugenol (**Eu**) under the catalysis of $H_2PtCl_6$ in the presence of isopropanol.[56] This reaction allowed the Si–H bonds of **PMHS** to react with the vinyl moiety of **Eu**, affording **Eu-PMHS** at room temperature in 72 h. Subsequently, **Eu-PMHS** was grafted onto **GO** through an esterification reaction. To do so, **GO** was first subjected to a chlorination reaction with thionyl chloride ($SOCl_2$) at 70 °C for 48 h, which converted the carboxyl groups of **GO** into acyl chlorides. The $SOCl_2$ treated **GO** was then subjected to esterification with **Eu-PMHS** in the presence of DMAP as a catalyst and tetrahydrofuran (THF) as a solvent at 80 °C for 24 h. This step led to the formation of an ester linkage between the **Eu** moiety of **Eu-PMHS** and the **GO** substrate, affording **Eu-PMHS-GO** as a black solid.

IR spectroscopic analysis confirmed the formation of **Eu-PMHS** and **Eu-PMHS-GO**. As shown in Fig. 3, the IR spectrum of **Eu-PMHS** (blue trace) shows the characteristic stretching modes of O–H (*ca.* 3500 $cm^{-1}$), C–H (3100–2800 $cm^{-1}$), and aromatic C=C (1610 $cm^{-1}$) bonds, all agreeing with the molecular structure of **Eu-PMHS**. Additionally, two significant peaks can be observed at 1085 and 1015 $cm^{-1}$, which correspond to the C–O stretching frequencies of ester groups. It is worth noting that the starting materials, **PMHS** and **Eu**, would show characteristic Si–H stretching at *ca.* 2100 and C=C stretching

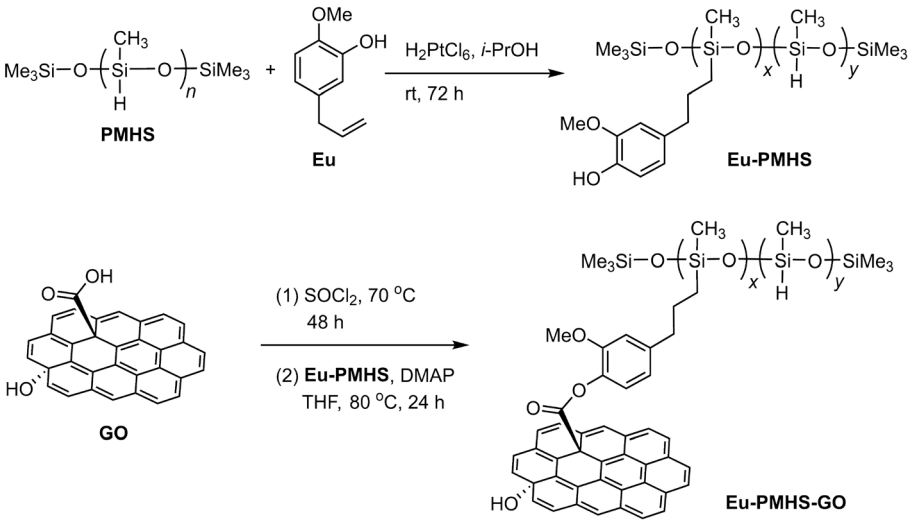


Fig. 2 Chemical synthesis of **Eu-PMHS** and **Eu-PMHS-GO**.

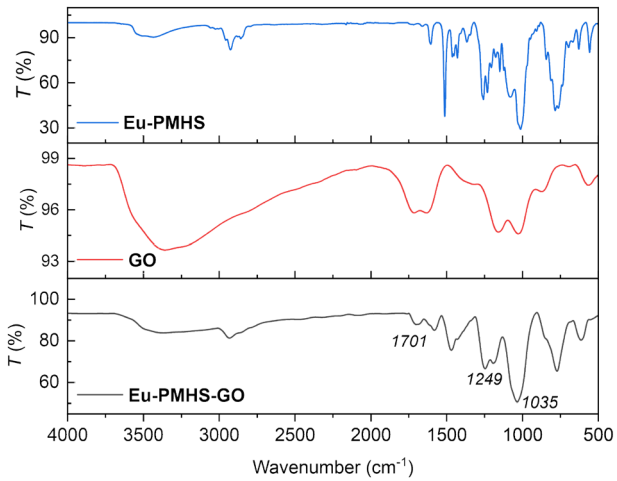


Fig. 3 IR spectra of **Eu-PMHS**, **GO**, and **Eu-PMHS-GO**.

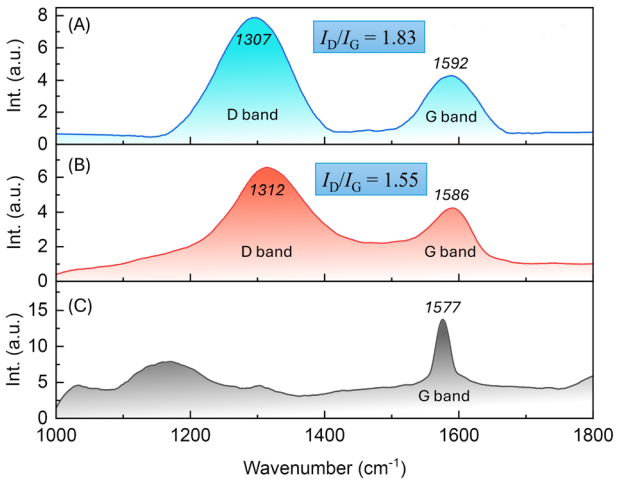


Fig. 4 Raman spectra showing the G- and D-bands of (A) **Eu-PMHS-GO**, (B) **GO**, and (C) graphite.

at 1650 $cm^{-1}$, respectively. These two bands are absent from the IR spectrum of **Eu-PMHS**, attesting to the efficiency of the Pt-catalyzed hydrosilylation reaction that converts them into Si–C and C–C bonds, respectively.

The IR spectrum of **GO** (red trace) features a broad O–H stretching band in the range of 3700 to 2500 $cm^{-1}$, which is predominantly attributed to the hydrogen-bonded carboxyl groups on **GO**. Furthermore, there are two significant IR bands at 1718 and 1639 $cm^{-1}$, which are due to the stretching of the C═O groups and graphitic C═C bonds of **GO**, respectively. In the IR spectrum of **Eu-PMHS-GO** (black trace), the O–H band appears in the range of 3600–2700 $cm^{-1}$ with a much weaker intensity, indicating the presence of residual hydroxyl groups after the esterfication. There is a pronounced C═O stretching band at 1701 $cm^{-1}$, which is slightly shifted to the low-frequency direction relative to the C═O peak of **GO**. Moreover, there are two significant peaks at 1249 and 1035 $cm^{-1}$, which can be assigned to the C–O vibrational pattern of ester. The IR analysis clearly confirms that **GO** was efficiently converted into **Eu-PMHS-GO** through the esterfication approach.

The molecular structures of **Eu-PMHS-GO** were further characterized using Raman spectroscopy, a technique particularly well-suited for analyzing graphitic structures and their functional modifications.[65] As illustrated in Fig. 4A, the spectrum of **Eu-PMHS-GO** exhibits two distinct graphitic bands at 1592 and 1307 $cm^{-1}$, respectively. Comparison to the spectrum of graphite (Fig. 4C) reveals that the first band is the G band of graphite, while the latter one is assigned to the D band, which is known as the disorder band or the defect band. The intensity ratio of these two bands ($I_G/I_D$) is 1.83, reflecting a high degree of covalent functionalization in the **GO** structure. The Raman spectrum of **GO** (Fig. 4B) indicates an $I_G/I_D$ value of 1.55, which is notably less than that of **Eu-PMHS-GO**. The result indicates that the functionalization reaction of **GO** with **Eu-PMHS** led to increased disorder in the graphene framework of **GO**. Overall,

the Raman and IR analyses congruously point to a high degree of covalent functionalization of **GO** through the esterification reaction with **Eu-PMHS**.

### Characterization of epoxy coatings modified with Eu-PMHS-GO

The prepared epoxy coatings incorporating with various amounts of **Eu-PMHS-GO** as additives did not show significant differences by visual check compared to the film of neat epoxy resin. However, SEM imaging analysis reveals notable morphological changes in the cross sections of epoxy coatings as the concentration of **Eu-PMHS-GO** increases. At low concentrations (0.001–0.005 wt%, Fig. 5A and B), the coatings appear to be relatively smooth with minor undulations and few particles, indicating minimal influence from the additives. As the concentration rises (0.01–0.05 wt%, Fig. 5C and D), surface roughness increases, with more pronounced ridges and valleys, suggesting a moderate interaction between the additives and the epoxy matrix. Further increases in additive concentration (0.1–0.5 wt%, Fig. 5E and F) lead to a more rugged surface with distinct features, highlighting the additives' role in promoting texture formation during curing. At higher concentrations (Fig. 5D), agglomeration and clustering of particles become evident, likely due to incomplete dispersion of the **Eu-PMHS-GO** additive, which may compromise coating uniformity and mechanical properties. Overall, the progression from smooth to more textured surfaces demonstrates the significant influence of **Eu-PMHS-GO** on the epoxy coating's morphology, with optimal concentrations likely balancing coating uniformity and additive-induced performance (*e.g.*, anticorrosion and antifouling effects).

The effect of **Eu-PMHS-GO** on the wettability of epoxy coatings was investigated through water contact angle (WCA) measurements, as illustrated in Fig. 6. The unmodified epoxy coating exhibits a WCA of 51° (Fig. 6A), indicating a hydrophilic surface with good wettability, allowing water to spread easily. Upon the addition of **GO** at 0.01 wt%, the WCA increases to 89.5° (Fig. 6B), reflecting a shift toward hydrophobicity. This change is attributed to the inherent hydrophobic nature of the graphene unit in **GO**, which reduces the surface's affinity for water.

For epoxy coatings modified with **Eu-PMHS-GO** (Fig. 6C to H), the WCA values range from 111 to 75°, demonstrating a progressive change of the coating surface from hydrophobic to hydrophilic in nature. Of particular note is that the WCA exhibits a decreasing trend with increasing weight percentage of **Eu-PMHS-GO** in the epoxy coating. The highest WCA of 111.2° corresponds to the lowest additive loading (0.001 wt%), indicating the most hydrophobic surface among the tested samples. This result aligns with SEM observations, suggesting that at low additive concentrations, the **Eu-PMHS-GO** additive is well dispersed within the void spaces of the epoxy polymer networks, resulting in effective blockage of the microchannels for water penetration and hence enhancing the coating's water resistance. In contrast, higher additive concentrations introduce structural defects and additive agglomerates in the coating, which negatively impacts the water resistance of the coating. Collectively, the SEM and WCA analyses demonstrate that the concentration of **Eu-PMHS-GO** plays a critical role in tailoring the wettability of epoxy coatings. The observed trend of WCAs points to an optimal loading of **Eu-PMHS-GO** at 0.001 wt% to achieve the best protective performance against corrosion and fouling.

To evaluate the mechanical properties of epoxy coatings modified with **Eu-PMHS-GO**, two critical parameters–tensile strength ($\sigma$) and nominal fracture strain ($\varepsilon_n$)–were measured. Herein, $\sigma$ refers to the maximum stress that a material can

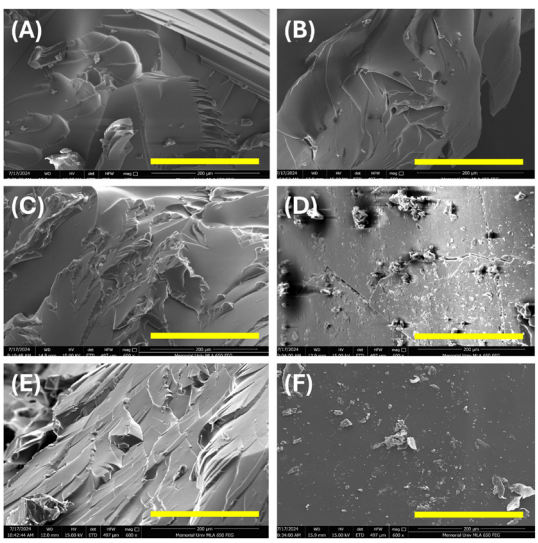


Fig. 5 SEM images of the cross-sectional morphology of epoxy coating films incorporating **Eu-PMHS-GO** at varying weight percentages: (A) 0.001 wt%, (B) 0.005 wt%, (C) 0.01 wt%, (D) 0.05 wt%, (E) 0.1 wt%, and (F) 0.5 wt%. A yellow scale bar indicates the length of 20 μm.

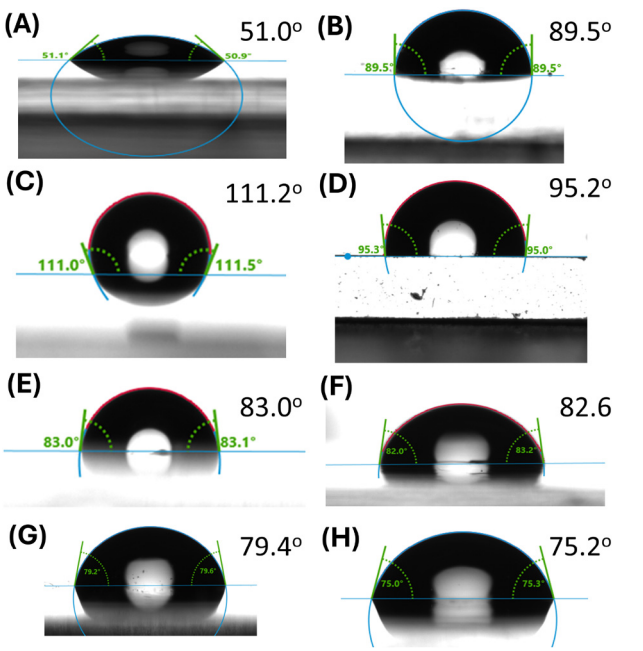


Fig. 6 Contact angle measurements on different epoxy coating surfaces. (A) epoxy, (B) epoxy + **GO** (0.01 wt%), (C) epoxy + **Eu-PMHS-GO** (0.001 wt%), (D) epoxy + **Eu-PMHS-GO** (0.005 wt%), (E) epoxy + **Eu-PMHS-GO** (0.01 wt%), (F) epoxy + **Eu-PMHS-GO** (0.05 wt%), (G) epoxy + **Eu-PMHS-GO** (0.1 wt%), and (H) epoxy + **Eu-PMHS-GO** (0.5 wt%).

Table 1 Mechanical properties of epoxy coatings without and with additives at 0.001 wt% concentration

| Additive | $\sigma$ (MPa) | $\varepsilon_n$ (%) |
|---|---|---|
| None | 169.4 | 2.6 |
| **GO** | 176.8 | 4.2 |
| **Eu-PMHS-GO** | 197.0 | 4.1 |

withstand while being stretched or pulled before necking, which is the point at which the material's cross-section starts to significantly contract. In the context of polymer coatings, a higher $\sigma$ value indicates a more robust and durable coating that can resist cracking and failure under tension. On the other hand, $\varepsilon_n$ is the strain at which a material breaks under tension. It is an indication of the material's ductility; that is, the ability to undergo significant plastic deformation before failure. For polymer coatings, a higher $\varepsilon_n$ suggests that the coating can stretch more before breaking, which can be particularly important for applications where the coating may be subjected to mechanical stress or deformation, such as in harsh marine environments.

Table 1 presents the measured $\sigma$ and $\varepsilon_n$ values for three epoxy coatings: unmodified epoxy, epoxy modifed with 0.001 wt% of **GO**, and epoxy modified with 0.001 wt% of **Eu-PMHS-GO**. The unmodified epoxy coating exhibits the lowest mechanical performance, while addition of **GO** and **Eu-PMHS-GO** significantly enhances both strength and ductility. Notably, **Eu-PMHS-GO** demonstrates a more pronounced improvement in $\sigma$ compared to **GO**, suggesting that the polysiloxane moiety in **Eu-PMHS-GO** further enhances the coating's robustness. In terms of $\varepsilon_n$, both **GO** and **Eu-PMHS-GO** show similar enhancement effects, indicating that the graphene component primarily drives the increased ductility of the coating. These results highlight the synergistic role of graphene and polysiloxane in improving the mechanical properties of epoxy coatings, with **Eu-PMHS-GO** offering superior strength while maintaining high ductility.

### Tolerance of Eu-PMHS-GO-modified epoxy coatings to environmental factors

To evaluate the environmental tolerance of epoxy coatings modified with 0.001 wt% **Eu-PMHS-GO**, we conducted time-dependent WCA measurements under a range of stress conditions, including thermal treatment at 100 °C, UV irradiation at 365 nm (5 mW $cm^{-2}$), and immersion in aqueous solutions of varying pH (3, 7, and 10). The WCA serves as a sensitive indicator of the coating's structural integrity and water-resistance performance, both of which are essential for its protective function.

As shown in Fig. 7, the modified epoxy coating initially displayed a high WCA of approximately 112°, demonstrating significant surface hydrophobicity and suggesting excellent barrier properties. Under thermal aging at 100 °C, the WCA declined moderately to 90° within the first 6 days, after which it stabilized and remained nearly constant over the subsequent 9 days. This relatively small decrease implies that the coating can maintain its structural integrity under prolonged heat exposure.

UV irradiation induced a slightly more pronounced decline in WCA, reaching 86° by day 9, after which no further significant

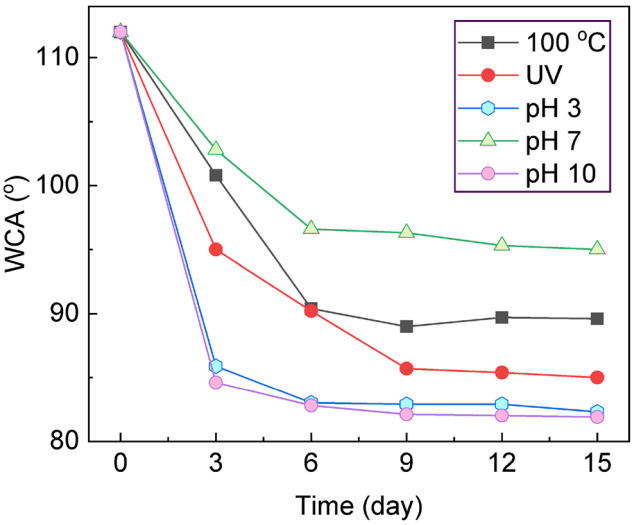


Fig. 7 Changes in contact angles for the epoxy coating modified with **Eu-PMHS-GO** (0.001 wt%) under different environmental conditions.

change was observed. The gradual nature of this decrease suggests some degree of photoinduced degradation or oxidation on surface, yet the coating still preserved notable hydrophobicity, attesting to its performance of resisting UV-induced aging.

In neutral aqueous conditions (pH 7), the WCA decreased to 97° over 6 days and then plateaued, indicating limited water ingress and minimal hydrolysis effects under these conditions. However, in acidic (pH 3) and alkaline (pH 10) environments, the WCA dropped more sharply to about 83°, suggesting that extreme pH levels are more aggressive toward the epoxy coating and **Eu-PMHS-GO** additive. The barely changed WCAs after 6 days of immersion suggest that the degradation reached equilibrium, probably associated with surface hydrolysis of both the epoxy matrix and the **Eu-PMHS-GO** additive.

Comparative analysis of these conditions indicates that chemical degradation under acidic and basic environments exerts the most significant impact on the surface properties of the coating, likely due to pH-driven cleavage of siloxane and epoxy bonds. Nevertheless, even under the harshest conditions tested, the WCA values remained substantially higher than those of unmodified epoxy coatings, indicating that the incorporation of **Eu-PMHS-GO** in the epoxy coating imparts enhanced environmental resilience. These results also demonstrate that the **Eu-PMHS-GO** additive not only reinforces the hydrophobic character of the epoxy coating but also effectively mitigates environmental degradation pathways, particularly in thermal and photochemical settings. The **Eu-PMHS-GO** additive is therefore expected to show strong promise for protective applications in environments where temperature fluctuations, UV exposure, and pH extremes are prevalent.

### Anticorrosion properties of epoxy coatings modified with Eu-PMHS-GO

Systematic experimental analyses were performed on **Eu-PMHS-GO**-modified epoxy coatings to evaluate their anticorrosion properties in seawater. Fig. 8 illustrates the experimental

outcomes of an immersion test, where the epoxy coatings modified with varying concentrations of **Eu-PMHS-GO** additive after 90 days of seawater immersion. The control sample, lacking **Eu-PMHS-GO**, exhibited significant corrosion with extensive rust formation around the scratched mark, underscoring the limited inherent resistance of the neat epoxy coating. The extent of corrosion was further assessed by examining the substrate and coating after peel-off. The steel surface exhibited widespread rust formation (panel B, Fig. 8), demonstrating that after electrolyte penetration through the scribe, corrosive attack progressed unabated at the interface. The corroborating evidence was found on the adhesive side of the epoxy coating, which showed visible rust diffusion (panel C, Fig. 8), confirming that corrosion propagation occurred beneath the coating layer. As the additive concentration was increased from 0.001 to 0.500 wt%, a clear trend of reduced anticorrosion performance was observed, characterized by increased rust formation and degraded coating surfaces around the scratched marks. Notably, the lowest concentration tested (0.001 wt%) provided the best corrosion resistance, aligning with prior findings that this loading optimizes structural integrity and water resistance, as supported by SEM imaging and WCA analyses. After the coating was removed, visual and microscopic inspection of the steel substrate revealed a very low degree of corrosion around the scribe mark, indicating highly effective protection. Intriguingly, the scratch on the epoxy surface appeared to be partially closed or "self-healed", suggesting **Eu-PMHS-GO** facilitated a recovery process. The lack of significant rust diffusion within the polymer matrix further confirms the coating's resilience against corrosive species ingress. Higher additive concentrations ($>0.01$ wt%) resulted in similarly low anticorrosion performance, comparable to that of the control sample. These findings highlight that **Eu-PMHS-GO** enhances the anticorrosion properties of epoxy coatings in a dose-dependent manner, with optimal performance achieved at low concentrations (0.001 wt%), where a balance between additive efficacy and the structural integrity of the polymer matrix is maintained.

To elucidate the anticorrosion mechanism of **Eu-PMHS-GO** as additive in epoxy coatings, EIS analyses were performed on three coatings–neat epoxy, epoxy with **GO** (0.001 wt%), and epoxy with **Eu-PMHS-GO** (0.001 wt%)–before and after immersion in seawater for varying durations. Fig. 9 presents the EIS plots measured from these coatings before and after 30 days of seawater immersion, revealing significant differences in their protective capabilities against corrosion. The epoxy coating modified with **Eu-PMHS-GO** demonstrates superior initial and sustained impedance values, indicating a higher charge transfer resistance and thus better corrosion resistance. Specifically, in the Bode impedance plots (Fig. 9A), the epoxy/**Eu-PMHS-GO** coating can be seen to exhibit impedance values in the low frequency region approximately two orders of magnitude higher than epoxy and epoxy/**GO** coatings before immersion. After 30 days of immersion in seawater, the impedance values of all three coatings decrease as a result of water and other corrosive agents (*e.g.*, electrolytes) entering into the coating layer. However, the impedance of epoxy/**Eu-PMHS-GO** still maintain a much higher level relative to those of epoxy and epoxy/**GO** coatings. This enhanced performance is also evident in the Nyquist plots (Fig. 9E and F). Even after 30 days, the epoxy/**Eu-PMHS-GO** coating retained a considerably larger semicircle diameter, whereas the neat epoxy and epoxy/**GO** coatings showed significantly smaller semicircles compared to their initial states. These results point to a synergistic effect between **Eu-PMHS** and **GO**, which is conducive to improved charge transfer resistance and long-term durability.

The Bode phase angle plots (Fig. 9B) of the three epoxy coatings show strong capacitive behavior at high frequencies for all three epoxy coatings before seawater immersion. In the low-frequency region, epoxy/**Eu-PMHS-GO** exhibits phase angles approaching $-90^{\circ}$, indicative of excellent barrier properties.

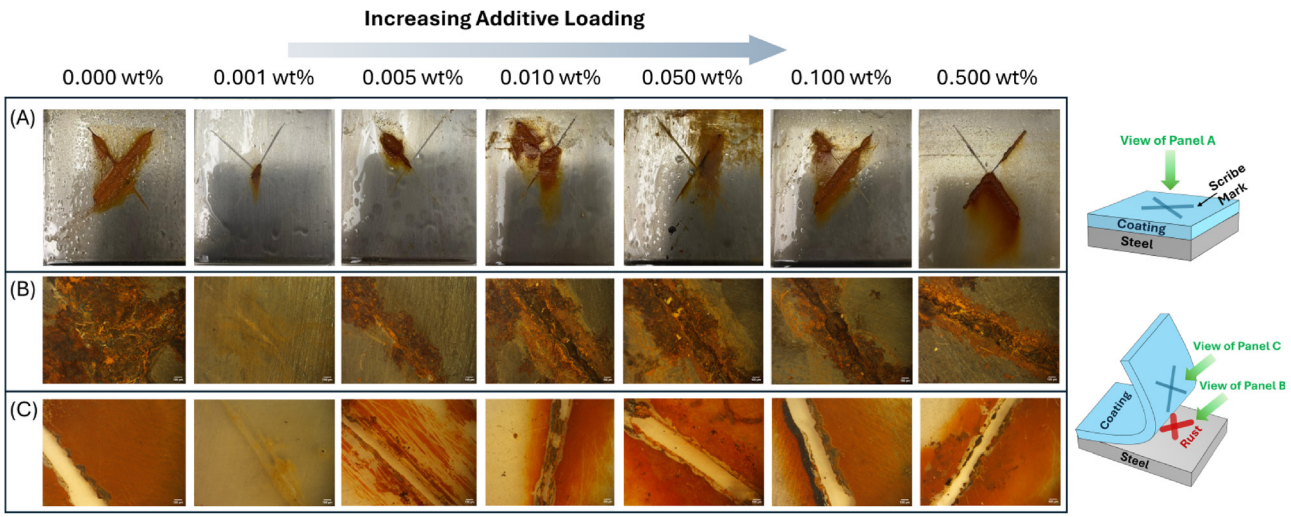


Fig. 8 Photographic images of scratched epoxy-coated carbon steels after immersion in seawater for 90 days. The weight percent loadings of **Eu-PMHS-GO** are indicated. Panel A: top surface of the intact coating around the scribe mark; panel B: exposed steel (around the scribe mark) after coating removal; panel C: adhesive side of the peeled coating (around the scribe mark).

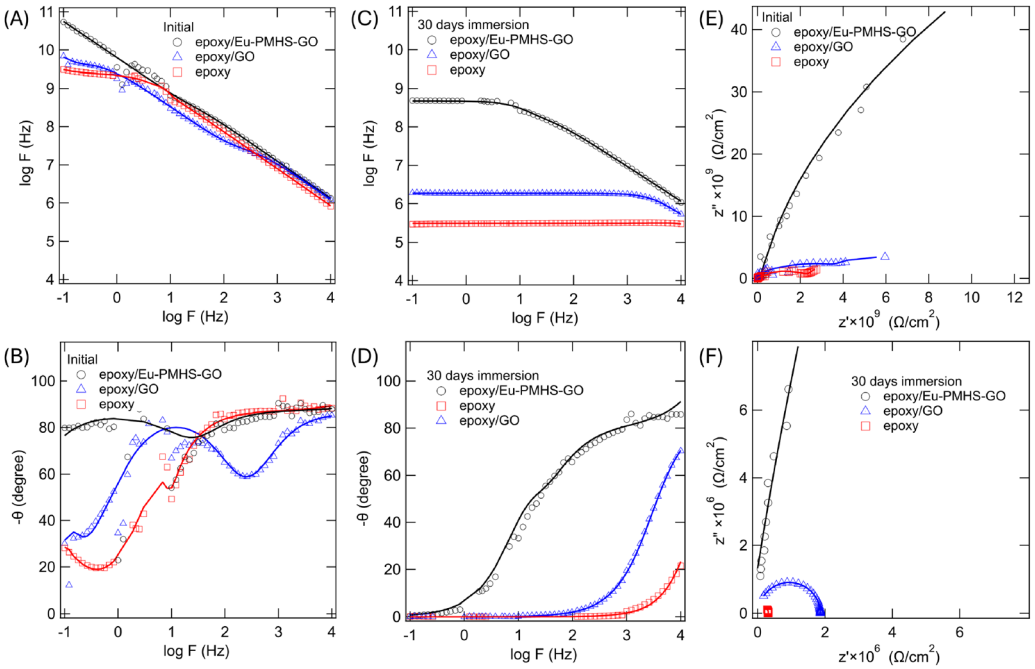


Fig. 9 (A) Bode impedance plots and (B) Bode phase angle plots for epoxy coatings on steel plates before immersion in seawater. (C) Bode impedance plots and (D) Bode phase angle plots for epoxy coatings on steel plates after immersion in seawater for 30 days. Nyquist plots for epoxy coatings on steel plates (E) before and (F) after immersion in seawater for 30 days. Measurements were done on three coatings: epoxy without any additives, epoxy with **GO** (0.001 wt%), and epoxy with **Eu-PMHS-GO** (0.001 wt%).

Conversely, the neat epoxy and epoxy/**GO** coatings show phase angles closer to 0°, suggesting a greater influence of diffusion processes. After 30 days of immersion, the phase angle plots of all coatings change significantly (Fig. 9D). The neat epoxy coating predominantly exhibits phase angles near 0°, indicating substantial water and electrolyte penetration and the onset of corrosion at the coating/metal interface. The epoxy/**GO** coating performs better in the high-frequency region, but its mid- and low-frequency phase angles are similar to those of neat epoxy coating. After 30 days of immersion, the epoxy/**Eu-PMHS-GO** coating maintains phase angles near 90° in the high-frequency region, gradually shifting toward 0° at low frequencies. The observations clearly demonstrate that modification of the epoxy coating with **Eu-PMHS-GO** can significantly enhance the structural integrity and barrier effects of the epoxy coating.

The EIS data for the epoxy coatings were further examined through fitting with electrochemical equivalent circuit (EEC) models to gain deeper insights into the coatings' anticorrosion mechanisms. Fig. 10 illustrates the detailed fitting results, in which four different EEC models were used to accurately fit the impedance data. Prior to immersion, all three coatings demonstrated high corrosion resistance, as evidenced by their large corrosion resistance values ($R_{corr} > 10^9$ Ohm). In particular, the coating modified with 0.001 wt% **Eu-PMHS-GO** exhibited the highest resistance, with an $R_{corr}$ value of $4.67 \times 10^{11}$ Ohm. The incorporation of 0.001 wt% **GO** as additive into the epoxy coating resulted in an $R_{corr}$ of $4.93 \times 10^9$ Ohm. While this value is two orders of magnitude lower than that of the **Eu-PMHS-GO**-modified coating, it is about two times larger than that of the neat epoxy coating ($2.34 \times 10^9$ Ohm). Following 30 days of immersion, the **Eu-PMHS-GO**-modified epoxy maintained excellent protective properties, retaining a high $R_{corr}$ of $2.73 \times 10^8$ Ohm. The **GO** modified coating showed a significantly reduced $R_{corr}$ of $9.78 \times 10^8$ Ohm, indicating a substantial decline in its protective performance. The neat epoxy coating, in contrast, exhibited a complete loss of corrosion resistance. The corresponding equivalent circuit data suggest the formation of major defects and delamination at the coating/metal interface, confirming a failure of its protective function. The EEC results clearly demonstrate that the **Eu-PMHS-GO** nanocomposite, at its optimal loading (0.001 wt%), endows the epoxy coating with a superior anticorrosion function, enabling robust protection both initially and during long-term seawater exposure.

In addition to the results discussed above, we monitored the detailed changes in EIS of the epoxy coatings over varying immersion periods (see the SI for detailed data). Fig. 11 summarizes the time-dependent changes in impedance ($Z$) and open circuit potential (OCP) of the epoxy coatings during immersion. The data illustrate the evolution of the coatings' electrochemical behavior, detailing the trends of their decreasing protective performance and degradation mechanisms over time. Our results confirm that the neat epoxy coating provides only a short-term protective effect, with significant corrosion (negative OCP) initiating at the coating/metal interface within a few days of immersion. In contrast, the incorporation of **GO** into the epoxy matrix extends the anticorrosion performance to approximately two weeks. Notably, the use of **Eu-PMHS-GO** as an additive gives rise to the most prolonged protective effect. Even after 30 days of immersion in seawater, the coating's electrochemical behavior continues to exhibit robust corrosion resistance, as evidenced by the electrochemical data.

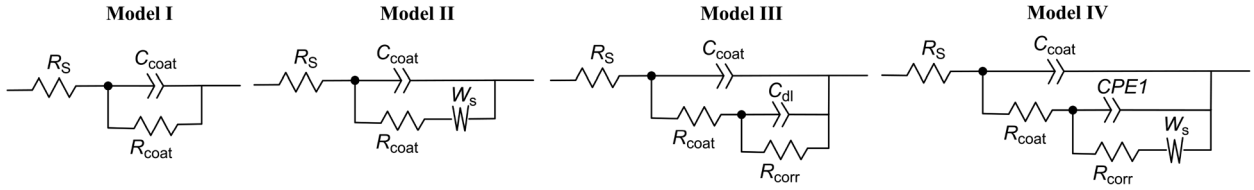


| Coating | Time (day) | Model | $R_s$ (Ohm) | $C_{coat\text{-}T}$ (F) | $C_{coat\text{-}P}$ | $R_{coat}$ (Ohm) | $C_{dl\text{-}T}$ (F) | $C_{dl\text{-}P}$ | $R_{corr}$ (Ohm) | $W_{s\text{-}R}$ (Ohm) | $W_{s\text{-}T}$ (s) | $W_{s\text{-}P}$ |
|---|---|---|---|---|---|---|---|---|---|---|---|---|
| 1 | 0 | I | $1.89 \times 10^{5}$ | $2.63 \times 10^{-11}$ | 0.92 | | | | $4.67 \times 10^{11}$ | | | |
| | 30 | III | $5.70 \times 10^{4}$ | $3.06 \times 10^{-11}$ | 0.93 | $2.04 \times 10^{8}$ | $4.41 \times 10^{-11}$ | 0.94 | $2.73 \times 10^{8}$ | | | |
| 2 | 0 | IV | $1.69 \times 10^{4}$ | $1.74 \times 10^{-11}$ | 0.97 | $3.69 \times 10^{7}$ | $3.97 \times 10^{-11}$ | 0.95 | $4.93 \times 10^{9}$ | $1.16 \times 10^{10}$ | 7.8 | 0.89 |
| | 30 | III | $4.36 \times 10^{3}$ | $1.11 \times 10^{-11}$ | 1.07 | $8.78 \times 10^{5}$ | $9.05 \times 10^{-11}$ | 0.89 | $9.78 \times 10^{5}$ | | | |
| 3 | 0 | II | $4.13 \times 10^{3}$ | $2.32 \times 10^{-11}$ | 0.98 | $2.34 \times 10^{9}$ | | | $2.34 \times 10^{9}$ | $1.03 \times 10^{10}$ | 15.58 | 0.84 |
| | 30 | I | $5.33 \times 10^{4}$ | | | | $6.61 \times 10^{-12}$ | 1.14 | $2.54 \times 10^{5}$ | | | |

Fig. 10 EECs and associated parameters used to fit the EIS data for various epoxy coatings before and after 30 days of immersion. Coating 1: epoxy with **Eu-PMHS-GO** (0.001 wt%); coating 2: epoxy with **GO** (0.001 wt%); coating 3: neat epoxy. $R_S$: resistance of electrolyte; $C_{coat\text{-}T/P}$: coating dielectric behavior; $R_{coat}$: coating resistance; $R_{corr}$: corrosion resistance; $C_{dl\text{-}T/P}$: double-layer behavior at the interface; $W_{s\text{-}R/T/P}$: diffusion/transport resistance and characteristics through coating defects.

## Erosion–corrosion analysis

To evaluate the stability and protective efficacy of our **Eu-PMHS-GO**-modified epoxy coating under dynamic conditions that simulate a harsh marine environment, erosion–corrosion tests were conducted where coatings were subjected to aqueous solutions containing NaCl and abrasive silica particles. They were maintained under constant stirring to create a synergistic erosion–corrosion effect, simulating the mechanical wear and electrochemical corrosion experienced by marine structures. SECM was used to directly probe the localized electrochemical activity of the coating surfaces before and after exposure to the erosive slurry for 24 and 72 h. The results, summarized in Fig. 12, reveal significant differences in the degradation mechanisms and anticorrosive effects of the neat epoxy coating in comparison with those modified with **GO** and **Eu-PMHS-GO**.

The neat epoxy coating exhibited a substantial loss of protective capability over time. The measured current response, a direct indicator of electrochemical activity, increased markedly from approximately 0.4 nA initially to 1.4 nA after 72 h. This nearly four-fold increase signifies a severe breakdown of the coating's barrier properties. The corresponding 3D SECM map (Fig. 12) further illustrates this degradation, showing pronounced surface heterogeneity and numerous sites of high local current. This morphology is characteristic of coating delamination, the formation of micropores, and the exposure of the underlying carbon steel substrate to the electrolyte, facilitating rapid corrosion.

Incorporating 0.001 wt% **GO** into the epoxy matrix led to a measurable improvement in performance. While an increase in current was still observed rising from 0.4 to 0.8 nA over 72 h, its progression was significantly less pronounced than in the neat epoxy. The final SECM map for this sample revealed a relatively smooth and homogeneous surface topography. This suggests that the well-dispersed **GO** nanosheets enhance the coating's integrity by creating a more tortuous path, which impedes the penetration of water, chloride ions, and abrasive particles. Such

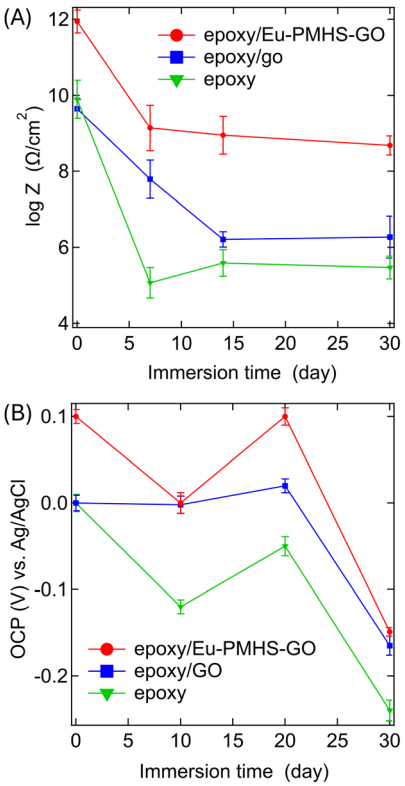


Fig. 11 Time-dependent changes in (A) impedance (log $Z$) and (B) OCP during immersion for various periods.

an effect results in enhanced barrier properties and delayed degradation under erosion–corrosion conditions.

The best performance was achieved by the coating modified with 0.001 wt% **Eu-PMHS-GO**, which imparted remarkable stability to the epoxy film. The current response showed only a minimal increase, from 0.4 to 0.57 nA over the 72-hour test, indicating consistently low electrochemical activity at the

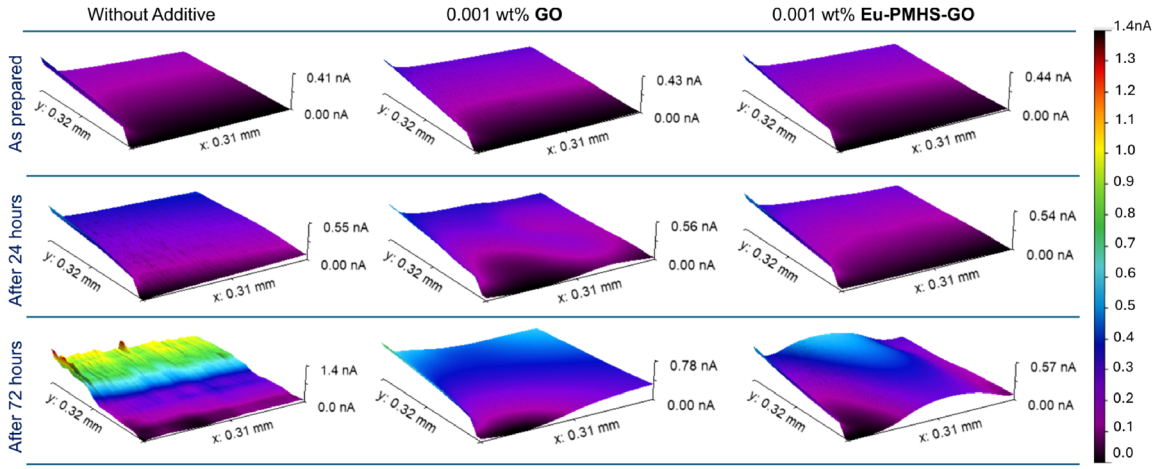


Fig. 12 SECM maps of epoxy-coated carbon steel during erosion–corrosion analysis. Coatings are without any additive (left column), modified with 0.001 wt% **GO** (middle column) and 0.001 wt% **Eu-PMHS-GO** (right column). Samples were immersed in a stirred aqueous solution of 3.5 wt% NaCl containing 20 wt% silica particles for varying durations.

surface. The homogeneity of the SECM map remained virtually unchanged, demonstrating that the coating retained its structural integrity. The superior performance of **Eu-PMHS-GO** is in line with the excellent mechanical properties of **Eu-PMHS-GO**-modified epoxy (*vide supra*) and can be attributed to a synergistic effect of the **GO**, **PMHS**, and **Eu** components, which offers active corrosion inhibition, possibly by passivating the underlying metal surface at defects, thereby providing protection against both erosion and corrosion.

### Anti-biofouling properties of epoxy coatings loaded with Eu-PMHS-GO

We first tested epoxy coatings containing **Eu-PMHS-GO** at concentrations ranging from 0.001 to 0.1 wt%, which were immersed in a culture of *P. tricornutum* for one week at 30 °C. After immersion, the density of clustered cells ($D$) on the surface of each coating was determined. As shown in Fig. 13, the surface of the neat epoxy coating was densely covered with *P. tricornutum*, exhibiting a $D$ value of 92.0%, which is a result of limited inhibitory effects on algal colonization. In contrast, the **Eu-PMHS-GO**-modified epoxy coatings demonstrated significantly improved anti-algal adhesion performance, with $D$ values ranging from approximately 4% to 12% at low loading percentages (0.001 to 0.05 wt%) and corresponding to inhibitory efficiencies of 95–87%. However, when the loading of **Eu-PMHS-GO** exceeded 0.1 wt%, the accumulation of *P. tricornutum* increased sharply to $D$ = 36% (0.1 wt% additive) and 74% (0.5 wt% additive), suggesting the emergence of additional influencing factors. Similar trends were observed in the adhesion tests conducted with the two bacterial species, *B. subtilis* and *Synechococcus* sp. (Fig. 13), where maximal inhibitory efficiencies achieved at 96% (0.001 wt% additive) and 86% (0.01 wt% additive).

The anti-biofouling performance of **Eu-PMHS-GO**-modified epoxy coatings, as demonstrated in this study, aligns with previous research highlighting the synergistic effects of **Eu** and **GO** in inhibiting microbial adhesion. **Eu**, a well-documented antimicrobial agent, disrupts microbial cell membranes and metabolic processes, contributing to the observed reduction in algal and bacterial adhesion.[66] Meanwhile, the incorporation of **GO** into the polymer matrix has been shown to enhance surface roughness and hydrophobicity, which can deter microbial attachment.[67] The concentration-dependent performance of **Eu-PMHS-GO** suggests that at low loadings (0.001–0.05 wt%), the additive effectively modifies the coating surface without causing aggregation, thereby maximizing antifouling efficacy. However, at higher concentrations (>0.1 wt%), the sharp increase in microbial adhesion may be attributed to increased aggregation of **Eu-PMHS-GO** on the coating surface, which could create microenvironments conducive to microbial colonization. Palmier *et al.* recently reported that **GO** shows complex bacterial interactions that could either inhibit or enhance bacterial growth on a surface.[68] To advance our **Eu-PMHS-GO** system toward practical anti-biofouling application, subsequent research must elucidate the concentration-dependent performance, long-term durability in real marine conditions, and environmental impact. The current anti-bacterial and anti-algal results establish a solid foundation for such development.

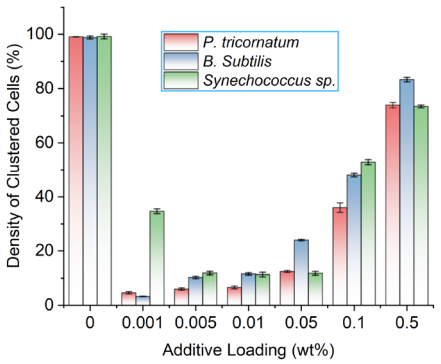


Fig. 13 Density of culstered cells determined on epoxy coating surface modified with varied amounts of **Eu-PMHS-GO** after one week.

**On the synergistic mechanisms of Eu-PMHS-GO**

Based on the experimental results, we propose that the superior performance of the **Eu-PMHS-GO** (0.001 wt%) modified epoxy coating in terms of anticorrosion and anti-biofouling efficacy can be attributed to a combination of complementary mechanisms working in concert:

1. Barrier protection *via* **GO** nanosheets: the nanometer-scale **GO** substrate ensures excellent dispersion in the epoxy resin, allowing the voids in the polymer matrix to be efficiently occupied. This forms a labyrinthine barrier that significantly hinders the diffusion of water, oxygen, and corrosive ions. The use of a low, optimal loading at 0.001 wt% is crucial to avoid agglomeration, which would disrupt the coating's structural integrity and reduce its protective quality.

2. Surface hydrophobicity and self-healing from **PMHS**: the **PMHS** chain significantly increases the coating's hydrophobicity. This water-repellent character minimizes surface wettability, which is a key first step in inhibiting microbial attachment and biofilm formation. Moreover, the hydrolyzable terminal groups of **PMHS** are hypothesized to facilitate a self-healing response; upon interaction with water, they can form a more dense, cross-linked network that seals micro-scratches, thereby recovering the barrier and enhancing long-term anticorrosion performance.

3. Inherent bioactivity from **Eu**: the **Eu** functional group delivers robust, intrinsic anti-bacterial and anti-algal properties. This bioactive component provides a direct chemical defense mechanism against microbial proliferation, complementing the physicochemical fouling-release properties afforded by hydrophobicity. Moreover, **Eu** exhibits strong surface affinity owing to its polar phenolic group, which in turn promotes effective binding at the additive–polymer interface, ensuring a stable and durable incorporation of **Eu-PMHS-GO** within the epoxy matrix. This strong binding effect helps to improve the mechanical strength and durability of the modified epoxy polymer, thereby ensuring long-term resistance corrosion and bio-accumulation.

## Conclusions

This study reports the design, synthesis, and application of a novel **Eu-PMHS-GO** nanocomposite, which serves as a multifunctional marine coating additive that synergistically combines the exceptional barrier properties of graphene oxide, the pronounced hydrophobicity and flexibility of polymethylhydrosiloxane, and the potent anti-biofouling activity of eugenol. This nanocomposite was incorporated into epoxy coatings at varying concentrations to evaluate its dual-functionality as an anticorrosion and anti-biofouling additive. Our studies demonstrated that **Eu-PMHS-GO** significantly enhanced the performance of epoxy coatings; particularly at a very low concentration (0.001 wt%), the modified coating exhibited improved hydrophobicity (WCA = 111.2°), mechanical strength ($\sigma$ = 197 MPa, $\varepsilon_n$ = 4.1%), and tolerance to environmental conditions such as heating, UV light, and pH. **Eu-PMHS-GO** acts as an efficient additive to prolong epoxy coating's corrosion resistance, as evidenced by immersion tests, EIS, and erosion–corrosion analyses. Notably, the coating maintained a high $R_{corr}$ of $2.73 \times 10^8$ Ohm even after 30 days of immersion in seawater, indicating robust, long-term barrier properties against corrosive

Table 2 Comparison of **Eu-PMHS-GO** with other **GO**, polysiloxane, and eugenol-based composite materials in marine coating application

| Coating System | Additive loading | Key properties | Application | Advantages | Ref. |
|---|---|---|---|---|---|
| **PDMS/GO**-$Al_2O_3$ | 1 wt% **GO**-$Al_2O_3$ | Superhydrophobic (WCA >150°), low SFE (12.4 mN $m^{-1}$), high mechanical strength | Ship hull antifouling | Eco-friendly, excellent stability, cost-effective | 33 |
| **PU-FPDMS Bu@PGMAm/GO** $[Zn(MIBA)_2]_n$ | 5 wt% $[Zn(MIBA)_2]_n$ | Broad-spectrum antifouling, controlled $Zn^{2+}$ release | Marine antifouling | Synergistic action, long-term efficacy (>180 days) | 69 |
| **PDMS/GO**-$Fe_3O_4$ | 1 wt% **GO**-$Fe_3O_4$ | Superhydrophobic (WCA: 158°), >95% microbial inhibition | Antifouling, anticorrosion | Bioinspired design, mechanical durability | 70 |
| Epoxy/**PDMS-GN** | 1 wt% **GN** | Modulus: 1570 MPa, tensile strength: 26.25 MPa, $T_g$: 77.6 °C | Protective coatings | Enhanced hydrophobicity, improved toughness | 71 |
| **PDMS/GO**-γ-AlOOH | 3 wt% **GO**-γ-AlOOH | WCA: 151°, strong interfacial adhesion | Marine antifouling | Superior dispersion, self-cleaning | 72 |
| Epoxy-**PDMS-GO** | 1 wt% **GO** | Corrosion rate: 0.0073 mm $year^{-1}$, 33.3% wear resistance improvement | Antifouling coatings | Synergistic effects, high thermal stability | 73 |
| **PE/Gr** | 1.25 wt% **Gr** | Barrier effect, corrosion inhibition: 78%, WCA: >90° | Copper anticorrosion | Biobased material, low-cost processing | 74 |
| **PDMS/GO**-$TiO_2$ | 1 wt% **GO**-$TiO_2$ | Photocatalytic activity, WCA: >150°, 90% *E. coli* inhibition | Marine/medical antifouling | Dual antifouling mechanism, biocompatible | 75 |
| Epoxy/**Eu** | 20 wt% **BMTO** | Anti-corrosion, anti-microbial properties, better film performance, bacterial adherence reduced by >90% | Metal surface coatings | Self-curing, strong adhesion, bio-based | 76 |
| BD/**PMES-Allyl** | 15 wt% **PMES-Allyl** | Impact and flexural strengths: 17.9 kJ $m^{-2}$ and 177.1 MPa, respectively | Thermosetting resin, harsh marine environment | Superior dispersion, better toughness, high thermal stability, and flame retardancy | 77 |
| Si-PC/**Gr** | 2.5 wt% **Gr** | WCA: 118.5°, tensile strength: 44.86 MPa, pyrolysis temperature: 434.3 °C | Marine equipment, packaging | High thermal stability, mechanical strength, and hydrophobicity | 60 |
| Epoxy/**Eu-PMHS-GO** | 0.001 wt% **Eu-PMHS-GO** | WCA: 111.2°, tensile strength: 197.0 MPa, nominal fracture strain: 4.1%, resistance to corrosion and erosion–corrosion, diatom and bacteria inhibition | Marine anticorrosion and antifouling | Dual function, long-term efficacy (90 days), bioinspired, self-healing, low-loading efficacy | This work |

media. In terms of anti-biofouling performance, incorporation of **Eu-PMHS-GO** at low concentrations (0.001–0.05 wt%) into epoxy coatings effectively inhibited the adhesion of marine microorganisms, including the diatom *P. tricornutum* and *B. subtilis* and *Synechococcus* sp. However, at higher concentrations (>0.1 wt%), the anti-algal and anti-bacterial performances are considerably reduced. These results underscore the importance of optimizing additive concentration to balance the protective effects of the coating in terms of anticorrosion and anti-biofouling. The synergistic effects of the antimicrobial properties of eugenol and the ability of graphene oxide and polysiloxane to enhance surface hydrophobicity and structural integrity contributed to the observed antifouling efficacy. As outlined in Table 2, our **Eu-PMHS-GO** clearly show advantages over other recently developed **GO**-based marine coatings across multiple key metrics. Whereas many reported coatings rely on high additive concentrations (>1 wt%) to impart properties like superhydrophobicity or antimicrobial activity, **Eu-PMHS-GO** delivers multifunctional anticorrosion, antifouling, and mechanical enhancement at a remarkably low loading of 0.001 wt%. This ultra-low concentration offers a substantial advantage by minimizing cost and simplifying processing while maintaining excellent performance. Moreover, the composite combines anticorrosion, antifouling, and self-healing properties, demonstrating a multifunctional and long-term synergy not typically attainable with a single additive. It also balances robust mechanical performance with hydrophobicity, outperforming composites that sacrifice structural robustness for improved surface characteristics. Our work therefore demonstrates the potential of **Eu-PMHS-GO** as a sustainable high-performance additive for marine coatings, addressing both corrosion and biofouling challenges in complex marine environments.

Beyond its outstanding performance, a key advantage of the **Eu-PMHS-GO** additive lies in its practical deployability. The nanocomposite can be seamlessly integrated into conventional marine coatings using established industrial methods, circumventing the need for costly reformulation or specialized application equipment. Its remarkably low optimal loading concentration of 0.001 wt% (equating to a mere 10 grams per metric ton of resin) points to exceptional cost-effectiveness for large-scale deployment. Furthermore, the incorporation of bio-based eugenol as a key component underscores the sustainable credentials of the **Eu-PMHS-GO** additive for advanced marine coatings. All these compelling attributes strongly warrant further investigation through pilot-scale production and rigorous field trials to comprehensively assess its potential in extending the service life of conventional marine coatings, reducing their maintenance frequency and environmental footprint.

## Conflicts of interest

There are no conflicts to declare.

## Data availability

The detailed electrochemical impedance spectroscopy (EIS) data and high-resolution photographic images of anti-algal (*Phaeodactylum tricornutum*) and anti-bacterial (*Bacillus subtilis*, *Synechococcus* sp.) adhesion tests for all epoxy coatings have been included as part of the supplementary information (SI). Supplementary information is available. See DOI: **https://doi.org/10.1039/d5ma01048a**.

## Acknowledgements

The authors acknowledge the Natural Sciences and Engineering Research Council of Canada (NSERC) and Canada Foundation for Innovation (CFI) for funding support. N. K. and L. N. thank the School of Graduate Studies, Memorial University of Newfoundland for providing them graduate scholarships.

## References

1 M. Abbas and M. Shafiee, *Mar. Struct.*, 2020, **71**, 102718.
2 P. Refait, A.-M. Grolleau, M. Jeannin, C. Rémazeilles and R. Sabot, *Corros. Mater. Degrad.*, 2020, **1**, 10.
3 Z. Wang, Z. Zhou, W. Xu, D. Yang, Y. Xu, L. Yang, J. Ren, Y. Li and Y. Huang, *Environ. Sci. Pollut. Res.*, 2021, **28**, 54403–54428.
4 B. J. Little, J. S. Lee and R. I. Ray, *Electrochim. Acta*, 2008, **54**, 2–7.
5 L. Procópio, *World J. Microbiol. Biotechnol.*, 2019, **35**, 73.
6 R. Ding, W. Li, X. Wang, T. Gui, B. Li, P. Han, H. Tian, A. Liu, X. Wang and X. Liu, *et al.*, *J. Alloys Compd.*, 2018, **764**, 1039–1055.
7 N. H. Othman, M. C. Ismail, M. Mustapha, N. Sallih, K. E. Kee and R. A. Jaal, *Prog. Org. Coat.*, 2019, **135**, 82–99.
8 G. Cui, Z. Bi, R. Zhang, J. Liu, X. Yu and Z. Li, *Chem. Eng. J.*, 2019, **373**, 104–121.
9 K. Ollik and M. Lieder, *Coatings*, 2020, **10**, 883.
10 B. Kulyk, M. A. Freitas, N. F. Santos, F. Mohseni, A. F. Carvalho, K. Yasakau, A. J. Fernandes, A. Bernardes, B. Figueiredo and R. Silva, *et al.*, *Crit. Rev. Solid State Mater. Sci.*, 2022, **47**, 309–355.
11 G. Jena and J. Philip, *Prog. Org. Coat.*, 2022, **173**, 107208.
12 A. K. Geim and K. S. Novoselov, *Nat. Mater.*, 2007, **6**, 183–191.
13 A. K. Geim, *Science*, 2009, **324**, 1530–1534.
14 M. J. Allen, V. C. Tung and R. B. Kaner, *Chem. Rev.*, 2010, **110**, 132–145.
15 L. Liao, H. Peng and Z. Liu, *J. Am. Chem. Soc.*, 2014, **136**, 12194–12200.
16 D. R. Dreyer, A. D. Todd and C. W. Bielawski, *Chem. Soc. Rev.*, 2014, **43**, 5288–5301.
17 Z. Sun, S. Fang and Y. H. Hu, *Chem. Rev.*, 2020, **120**, 10336–10453.
18 W. Chee, H. Lim, N. Huang and I. Harrison, *RSC Adv.*, 2015, **5**, 68014–68051.
19 O. C. Compton and S. T. Nguyen, *Small*, 2010, **6**, 711–723.
20 D. Chen, H. Feng and J. Li, *Chem. Rev.*, 2012, **112**, 6027–6053.
21 V. Georgakilas, J. N. Tiwari, K. C. Kemp, J. A. Perman, A. B. Bourlinos, K. S. Kim and R. Zboril, *Chem. Rev.*, 2016, **116**, 5464–5519.
22 A. Razaq, F. Bibi, X. Zheng, R. Papadakis, S. H. M. Jafri and H. Li, *Materials*, 2022, **15**, 1012.
23 Z. Li, Z. Liu, H. Sun and C. Gao, *Chem. Rev.*, 2015, **115**, 7046–7117.

24 R. Tarcan, O. Todor-Boer, I. Petrovai, C. Leordean, S. Astilean and I. Botiz, *J. Mater. Chem. C*, 2020, **8**, 1198–1224.
25 K. Krishnamoorthy, K. Jeyasubramanian, M. Premanathan, G. Subbiah, H. S. Shin and S. J. Kim, *Carbon*, 2014, **72**, 328–337.
26 D. S. Chauhan, M. Quraishi, K. Ansari and T. A. Saleh, *Prog. Org. Coat.*, 2020, **147**, 105741.
27 M.-I. Necolau and A.-M. Pandele, *Coatings*, 2020, **10**, 1149.
28 S. S. A. Kumar, S. Bashir, K. Ramesh and S. Ramesh, *Prog. Org. Coat.*, 2021, **154**, 106215.
29 W. Sun, L. Wang, T. Wu, Y. Pan and G. Liu, *Carbon*, 2014, **79**, 605–614.
30 R. D. Davidson, Y. Cubides, C. Fincher, P. Stein, C. McLain, B.-X. Xu, M. Pharr, H. Castaneda and S. Banerjee, *ACS Appl. Nano Mater.*, 2019, **2**, 3100–3116.
31 J. Lee, H.-R. Chae, Y. J. Won, K. Lee, C.-H. Lee, H. H. Lee, I.-C. Kim and J.-M. Lee, *J. Membr. Sci.*, 2013, **448**, 223–230.
32 S. Bano, A. Mahmood, S.-J. Kim and K.-H. Lee, *J. Mater. Chem. A*, 2015, **3**, 2065–2071.
33 M. S. Selim, S. A. El-Safty, N. A. Fatthallah and M. A. Shenashen, *Prog. Org. Coat.*, 2018, **121**, 160–172.
34 C. Yang, M. Long, C. Ding, R. Zhang, S. Zhang, J. Yuan, K. Zhi, Z. Yin, Y. Zheng and Y. Liu, *et al.*, *Nat. Commun.*, 2022, **13**, 7334.
35 J. Huang, D. Li, Z. Peng, B. Zhang, Y. Yao and S. Chen, *ACS Appl. Mater. Interfaces*, 2023, **15**, 43026–43037.
36 Z. Tang, B. Pan, P. Hao, S. Xu, Q. Li, L. Zhang and J. Lu, *Langmuir*, 2024, **40**, 26026–26032.
37 T. Shu, Y. Zhang, Y. Cao, F. Wang, B. Jiang, Y. Lei, L. Dong and X. Chen, *Chem. Eng. J. Adv.*, 2024, **18**, 100592.
38 J. Yu, S. Tian, G. Lu, S. Xu, K. Yang, L. Ye, Q. Li, L. Zhang and J. Yang, *Nano Lett.*, 2025, **25**, 987–994.
39 J. Zhu, L. Yuan, Q. Guan, G. Liang and A. Gu, *Chem. Eng. J.*, 2017, **310**, 134–147.
40 M. Hasani, M. Mahdavian, H. Yari and B. Ramezanzadeh, *Prog. Org. Coat.*, 2018, **116**, 90–101.
41 S. Amrollahi, B. Ramezanzadeh, H. Yari, M. Ramezanzadeh and M. Mahdavian, *Composites, Part B*, 2019, **173**, 106804.
42 N. Asim, M. Badiei, N. A. Samsudin, M. Mohammad, H. Razali, S. Soltani and N. Amin, *Composites, Part B*, 2022, **245**, 110188.
43 C. Ruücker and K. Kuümmerer, *Chem. Rev.*, 2015, **115**, 466–524.
44 U. Eduok, O. Faye and J. Szpunar, *Prog. Org. Coat.*, 2017, **111**, 124–163.
45 A. Pistone, C. Scolaro and A. Visco, *Polymers*, 2021, **13**, 173.
46 Y. Zhuo, S. Xiao, A. Amirfazli, J. He and Z. Zhang, *Chem. Eng. J.*, 2021, **405**, 127088.
47 A. Ribeiro, B. Soares, J. Furtado, A. Silva and N. Couto, *Prog. Org. Coat.*, 2022, **168**, 106867.
48 M. Zheng, L. Zhang and Y. Feng, *J. Mater. Sci.*, 2024, 1–21.
49 I. O. Arukalam, E. E. Oguzie and Y. Li, *J. Colloid Interface Sci.*, 2018, **512**, 674–685.
50 Y. Wei, F. Xu, L. Meng, C. Yu, D. Fu, Y. Chang, Y. Sun and H. Wang, *Prog. Org. Coat.*, 2022, **172**, 107131.
51 C. Zhang, J. Liang, Y. Yang, B. Liu, C. Cheng and C. Hu, *Mater. Chem. Phys.*, 2024, **325**, 129717.
52 D. Akuzov, T. Vladkova, G. Zamfirova, V. Gaydarov, M. V. Nascimento, N. Szeglat and I. Grunwald, *Prog. Org. Coat.*, 2017, **103**, 126–134.
53 X. Sun, R. Chen, X. Gao, Q. Liu, J. Liu, H. Zhang, J. Yu, P. Liu, K. Takahashi and J. Wang, *Eur. Polym. J.*, 2019, **117**, 77–85.
54 Z. Zhang, Q. Xie, G. Zhang, C. Ma and G. Zhang, *ACS Appl. Polym. Mater.*, 2023, **5**, 3524–3533.
55 S. Zhang, Y. Deng, B. Wu, Y. Yang, J. Chang, X. Zhang, B. Chen, B. Chen and J. Wu, *Colloids Surf., A*, 2025, **709**, 136095.
56 G. Chen, J. Feng, W. Qiu and Y. Zhao, *RSC Adv.*, 2017, **7**, 55967–55976.
57 R. Morales-Cerrada, S. Molina-Gutierrez, P. Lacroix-Desmazes and S. Caillol, *Biomacromolecules*, 2021, **22**, 3625–3648.
58 S. Caillol, B. Boutevin and R. Auvergne, *Polymer*, 2021, **223**, 123663.
59 B. Kumar, D. O. Agumba, D. H. Pham, H. C. Kim and J. Kim, *J. Appl. Polym. Sci.*, 2022, **139**, 51532.
60 X. Pang, M. Chen, J. Fu, Z. Lin, Y. Li, J. Wu, J. Yan, X. Chen and J. Ge, *Nanomaterials*, 2019, **9**, 1747.
61 G. Eyambe, L. Canales and B. K. Banik, *Heterocycl. Lett.*, 2011, **1**, 154.
62 M. Ulanowska and B. Olas, *Inter. J. Mol. Sci.*, 2021, **22**, 3671.
63 A. Marchese, R. Barbieri, E. Coppo, I. E. Orhan, M. Daglia, S. F. Nabavi, M. Izadi, M. Abdollahi, S. M. Nabavi and M. Ajami, *Crit. Rev. Microbiol.*, 2017, **43**, 668–689.
64 W. S. Hummers Jr and R. E. Offeman, *J. Am. Chem. Soc.*, 1958, **80**, 1339.
65 K. N. Kudin, B. Ozbas, H. C. Schniepp, R. K. Prud'Homme, I. A. Aksay and R. Car, *Nano Lett.*, 2008, **8**, 36–41.
66 T. A. N. Ribeiro, G. A. Dos Santos, C. T. Dos Santos, D. C. F. Soares, M. F. Saraiva, D. H. S. Leal and D. Sachs, *Microb. Pathog.*, 2024, 106937.
67 I. Levchenko, A. Kumar, A. AL-Jumaili, O. Bazaka, E. P. Ivanova, C. Riccardi, H. E. Roman, S. Xu, M. V. Jacob and O. Baranov, *et al.*, *Adv. Eng. Mater.*, 2024, **26**, 2300541.
68 V. Palmieri, F. Bugli, M. C. Lauriola, M. Cacaci, R. Torelli, G. Ciasca, C. Conti, M. Sanguinetti, M. Papi and M. De Spirito, *ACS Biomater. Sci. Eng.*, 2017, **3**, 619–627.
69 J. Liu, M. Rao, F. Xia, B. Jia, N. Zheng, H. Jiang, Z. Li, J. Lu, W. Li and G. Wang, *J. Mater. Sci. Technol.*, 2026, **250**, 40–52.
70 M. S. Selim, N. A. Fatthallah, M. A. Shenashen, S. A. Higazy, H. R. Madian, M. M. Selim and S. A. El-Safty, *Langmuir*, 2023, **39**, 2333–2346.
71 S. Verma, S. Das, S. Mohanty and S. K. Nayak, *J. Mater. Res.*, 2019, **34**, 2881–2894.
72 M. S. Selim, N. A. Fatthallah, S. A. Higazy, Z. Hao and P. J. Mo, *J. Colloid Interface Sci.*, 2022, **606**, 367–383.
73 S. Verma, S. Mohanty and S. Nayak, *Soft Matter*, 2020, **16**, 1211–1226.
74 N. B. A. Prasetya, A. I. Ajizan, D. S. Widodo, N. Ngadiwiyana and G. Gunawan, *Mater. Adv.*, 2023, **4**, 248–255.
75 M. S. Selim, A. M. Azzam, S. A. Higazy, S. A. El-Safty and M. A. Shenashen, *Prog. Org. Coat.*, 2022, **167**, 106803.
76 A. Patil, N. Pawar, P. Mali, M. Tayade, K. Borse and V. Patil, *Polym. Bull.*, 2025, 1–19.
77 Z. Zhang, K. Zhang, K. Xie, Y. Bao, X. Li, J. Huang, X. Li and W. Wei, *Eur. Polym. J.*, 2022, **180**, 111594.